Phantom Study of Breast Tissue Attenuation in Myocardial Imaging

Stephen H. Manglos, F. Deaver Thomas, George M. Gagne and Bradford J. Hellwig

Department of Radiology, SUNY Health Science Center, Syracuse, New York

The attenuation of photons by the breasts and other soft tissue overlying the chest may decrease the diagnostic accuracy of SPECT myocardial imaging. In this experiment, we measured the attenuation distortion of myocardial polar maps using a thorax phantom with a cardiac insert and added breast tissue. The distortion was measured using a regional semiquantitative analysis. Attenuation compensation was performed using a cone-beam radionuclide CT attenuation map. Breast tissue attenuation created apparent "defects" in the polar map, where the intensity was reduced by up to 35% relative to the most intense region. However, the size, location and severity of the reduction depended on cardiac insert orientation and breast placement. For the geometries studied, apparent "defects" were observed in the anterior wall, the apex, the inferior wall and basal regions. These results suggest that attenuation artifacts may occur in almost any location. However, the attenuation compensation nearly eliminated the apparent defects and improved polar map symmetry. After compensation, the variations between regions were generally 5% or less. Therefore, we expect that attenuation compensation will improve diagnostic accuracy in myocardial imaging in female patients and in males with excessive musculature or soft tissue. Without such compensation, diagnosis may be compromised.

J Nucl Med 1993; 34:992–996

It is well known that photon attenuation in SPECT may reduce quantitative accuracy (*1,2*) and distort images (*3–5*). In particular, myocardial SPECT images are distorted (*4,6–8*) by a complex and highly nonuniform attenuating geometry, which contains lungs, bones and soft tissue. The geometry is different for each patient and even depends upon patient positioning. For example, in the supine position, the diaphragm may attenuate the inferior wall of the myocardium (*7*).

Furthermore, breast tissue attenuation in females may produce artifacts in the anterior wall (*8*). These artifacts are highly dependent on breast size and whether or not the patient is wearing a bra, and they are difficult to distinguish from true perfusion defects. There is a corresponding loss of diagnostic confidence and a risk of false-positives, if the diagnostician ignores breast attenuation, and of false-negatives, if the effect is overestimated. Thus, at least for women with large breasts, it may be impossible to conclusively diagnose anterior wall defects.

Two other concerns are: (1) that the estimated size of true defects may be inaccurate if the normal data set used for quantitative comparison is much differently attenuated than the patient; and (2) that nonisotropic attenuation may produce localized image distortion ("streaks") (*3,5*).

Previously, there had been no easy clinical remedy to these artifacts. Attenuation compensation based on an average attenuation map is unlikely to be acceptable given the large variations in patient anatomy. Further, the anatomy is not well described by the simple, usually convex or elliptical, body contour used in most clinical attenuation compensation algorithms, nor is it well described by the assumed uniform map of attenuation coefficients. Therefore, clinicians have had to accept the reduction in diagnostic accuracy, while making subjective judgements on the likelihood of attenuation artifacts based upon breast size and any obvious artifacts in the projection set.

However, recent advancements in techniques to measure the attenuation map (*9–15*) and/or superimpose the corresponding x-ray CT image may allow for easier and more accurate correction of attenuation artifacts. These techniques can theoretically correct for all such artifacts, regardless of their cause: breast, lung, bones, diaphragm or other soft tissue. They are most likely to be useful in the human thorax, which is large and nonuniform.

Because some of these new techniques may become available clinically, this paper measures breast attenuation artifacts using a realistic phantom model of the myocardium in a thorax with added breast tissue, and it reports our attempts at attenuation compensation using a cone-beam radionuclide CT (CB-CT) attenuation map (*12,13,15*). The intensity, size and location of breast attenuation artifacts, before and after compensation, are reported for several anatomical variations.

METHODS

Acquisition and Reconstruction Protocols

Simulated breast tissue was added to a thorax model simulating lungs, spine and soft tissue of a realistic size and shape for a relatively small adult (32-cm diameter from left to right lateral).

Received Oct. 30, 1992; revision accepted Feb. 25, 1993.

For correspondence or reprints contact: Stephen H. Manglos, PhD, Department of Radiology, Physics Section, SUNY Health Science Center, 750 E. Adams St., Syracuse, NY 13210.

The breasts, as obtained from a RANDO phantom (Nuclear Associates, Carle Place, NY), were radiographically equivalent to soft tissue in the shape of right circular cones, 8 cm high and 14 cm wide at the base. A cardiac insert (Data Spectrum Corporation, Hillsborough, NC) simulated the myocardium of the left ventricle with no defects. Several orientations were used (see Table 1), but for each the insert was adjacent to the left lung and was obliquely oriented approximately halfway between the anterior and left lateral.

Each experiment consisted of a CB-CT acquisition (*12,13*) followed immediately by a SPECT acquisition with the phantom in the same position. The CB-CT provided the attenuation map for attenuation compensation of the SPECT data. All studies were acquired on a Siemens Orbiter gamma camera (Des Plaines, IL). SPECT and CB-CT acquisition matrices were 64 × 64 with 64 angular views covering 360°.

For CB-CT, a "point" transmission source was placed at the focal point of a long focal length (1 meter) cone-beam collimator (Von Gahlen, Didam, Holland). The point source was approximately a 5 × 5 mm cylinder with 2 mCi of ^{99m}Tc. The photons were imaged with an 18% energy window at 140 keV. During CB-CT, no activity was placed inside the phantom, although the cardiac insert itself was present. The radius of rotation of the circular orbit was 19 cm measured to the front of the cone-beam collimator. Total acquisition time was about 15 min. A clinical implementation might be able to use stronger point sources and much shorter acquisition times.

Given the moderate size and circular field of view of the gamma camera, image truncation was possible. Therefore, CB-CT reconstruction was performed with 80 iterations of a transmission maximum likelihood algorithm (TR-ML) (*16–17*), which partially reduces truncation artifacts. The reconstructed slice thickness was about 10 mm (32 TR-ML slices covering the focused cone-beam field of view). This reconstruction produces properly scaled and properly slice-dependent narrow beam attenuation coefficient maps in units of inverse centimeters. Truncation was further limited by placing the cardiac insert in the axial center of the gamma camera where the field of view is largest.

Immediately after the CB-CT acquisitions, the phantom was removed and 4.5 mCi of ^{99m}Tc was added to the myocardium of the insert. Both the phantom and the insert inside the phantom were returned to the original position and orientation, and SPECT acquisitions were performed with a LEAP collimator. The acquisition time was 5 min, which simulates a clinical acquisition of 20–30 min with 750 μCi in the myocardium.

SPECT reconstruction and attenuation compensation were performed with "attenuation-weighted filtered backprojection" (*18*) adapted to nonuniform attenuation maps (*19*). All parameters used are given elsewhere (*19*). For use in attenuation compensation, the attenuation maps were converted from narrow-beam to "effective" attenuation coefficients (*13,20*) by multiplying by 0.8. Thus, water had an "effective" coefficient of 0.8 × 0.15 = 0.12 cm^{-1}.

Analysis

After reconstruction, the SPECT slices were reoriented along the ventricle long-axis and polar maps were created using standard Cedars-Sinai software (*21*) on a Siemens MicroDelta. Semiquantitative analysis of the polar maps was performed using the regions shown in Figure 2. We report the activity of each region divided by the activity of the most active region. Each region contained about 10% of the polar map area, except for the two apex regions, which were smaller.

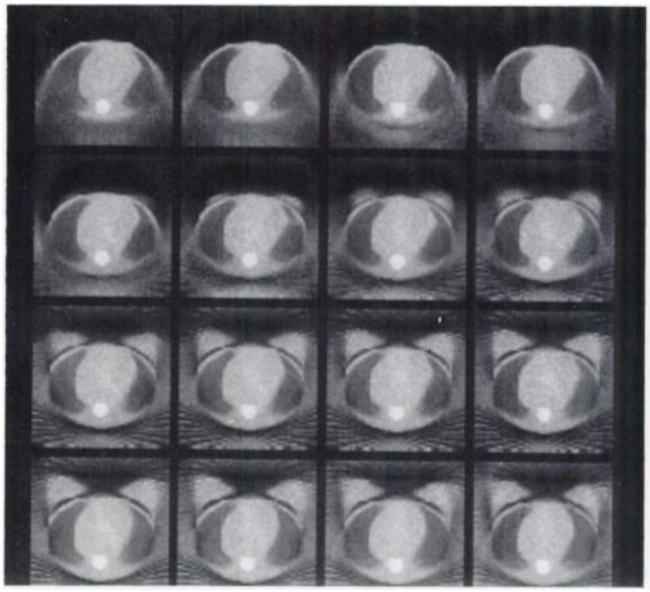

FIGURE 1. CB-CT of thorax phantom with breast tissue reconstructed with TR-ML. Sixteen slices containing the cardiac insert are shown. For each image, phantom left appears at observer right and vice versa. The upper left image is caudal to the insert and the bottom right image is cranial to the insert. The gray scale extends from 0.0 to 0.22 cm^{-1}.

RESULTS

SPECT attenuation compensation was performed using a CB-CT of the phantom. An example with breast tissue appears in Figure 1. Sixteen slices covering the region of the cardiac insert are shown. All relevant "organs" were clearly visible, including the lungs, spine and breasts. The plastic of the cardiac insert is partially visible (e.g., rightmost image in the second row), but it is not clear due to statistical noise and the relatively large pixel size. Truncation reduced the definition of the lateral and posterior body contour and erroneously placed density outside the body contour, especially posteriorly. (With our phantom holder, there was no table underneath these phantom slices.) These artifacts, however, were not severe. In contrast, cone-beam filtered backprojection (*22*) reconstructions (not shown) had more severe "streak" artifacts. These images were not used for attenuation compensation, since they created small artifacts in the polar maps. Comparison of truncation artifacts for the two reconstruction methods have been described elsewhere (*17*).

Figure 2 shows a polar map of the cardiac insert acquired in air (with no other attenuators than the insert itself). This image illustrates the normal statistical variations from the perfect symmetry present in the polar maps. It also illustrates a small apical decrease of about 10%, which appears worse in the anterior half of the apex. The apical decrease was present regardless of orientation or precise position of the insert. Although the insert had some self-attenuation, it cannot explain the apical decrease. In fact, for this orientation parallel to the axis of rotation, the apex was less self-attenuated than the rest of the phantom and it should thus appear more active. The decrease was also apparent

in long-axis sagittal and coronal slices, so it was not primarily due to the polar map generation process. The decrease was caused most likely by minor imperfections in the construction of the phantom. Nonetheless, the symmetry of the rest of the phantom appears adequate for these experiments.

The polar maps are illustrated in Figure 3, and Figure 4 provides the regional semiquantitative analysis for all four cases defined in Table 1. One experiment was performed for each case. When the thorax phantom was imaged without breasts (Case 1), attenuation decreased the inferior region of the polar map. As demonstrated by quantitative analysis, this region was about 15% lower than the most active region, which was at left lateral. With attenuation compensation using the TR-ML CB-CT attenuation map, the polar map was much more symmetric in appearance and the regional variations were no greater than 5%.

Case 2 modeled a common left ventricular orientation and breast location. An extended apparent anterior "defect" was 15%–20% reduced from the most active inferior region. In addition, the transverse slices (prior to oblique reorientation) showed "streak" artifacts (Fig. 5) in the background around the insert as well as nonuniformities in activity. Qualitatively, the insert appeared stretched in directions of decreased attenuation, and there were negative-activity artifacts in directions of increased attenuation (i.e., toward the breasts). These streaks are consistent with previously observed artifacts (*3,5*) due to nonisotropic attenuation. With attenuation compensation using the attenuation map in Figure 1, the polar map was more symmetrical, the anterior "defect" was removed and the streaks in the transverse slices were greatly reduced. In addition, the apex, especially on the anterior side, was reduced similarly to the "in air" polar map, although quantitative comparison was not possible due to the nonzero self-attenuation in the "in air" data.

Two less common physical geometries were also modeled to discover variations of attenuation effects. For Case 3, the insert was tilted caudally by 65° and the breasts covered the apex. Here, instead of the anterior region, the inferior region demonstrated a large apparent defect, which was decreased by 30%–35%. The apex was also similarly decreased, although this decrease was due to both attenuation and the assumed misconstruction of the phantom. With attenuation compensation, the polar map was much more symmetric. The largest variations between regions

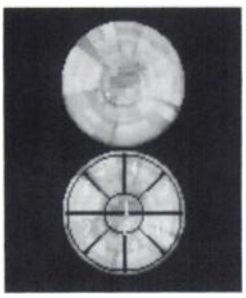

FIGURE 2. Polar map of cardiac insert in air. The bottom image defines the regions used in the quantitative analysis. Regions 1 and 2 contain the apex of the "myocardium." Regions 4 and 5 contain the anterior wall. Regions 6 and 7 contain the septal wall. Regions 8 and 9 contain the inferior wall. Regions 3 and 10 contain the lateral wall.

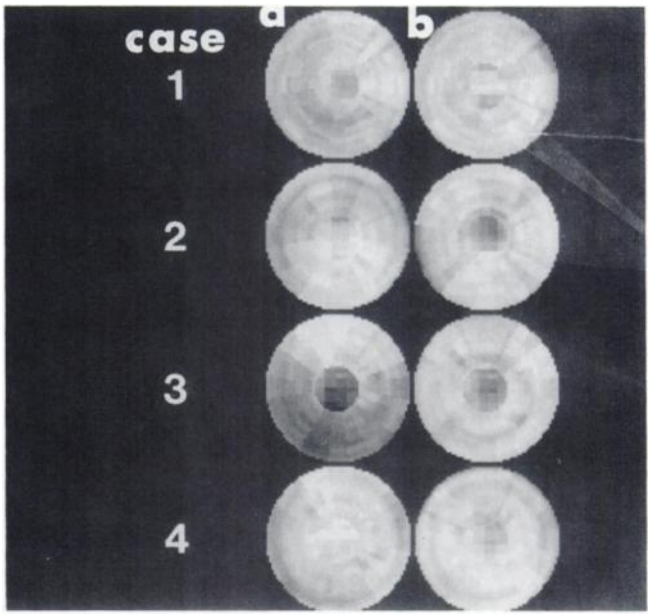

FIGURE 3. Polar map comparison for each case defined in Table 1. Uncompensated polar maps are in column A and attenuation compensated polar maps are in column B. The bottom of the gray scale was raised to 60% of the maximum to accentuate the apparent "defects." Each polar map has been separately normalized so that the maximum equals 100.

were about 5%, except for the apex, which was more decreased. This is in qualitative agreement with the "in air" polar map.

For Case 4, the insert was oriented the same way as in Case 3, but the breast was moved cranially so that it did not attenuate the apex. Here, the effects were more subtle, but the basal regions were decreased, especially inferiorly. The was no apparent decrease in the apex. With attenuation compensation, the polar map was again more symmetric and the apex was again decreased.

DISCUSSION

The simulated breast tissue used in this experiment greatly decreased the apparent circular symmetry in polar maps of the simulated myocardium. Asymmetries were as large as 30%–35%. The clinical effects may be larger, especially if the patient is much larger than our phantom and if ^{201}Tl is used instead of ^{99m}Tc. Thus, as is generally known clinically, breast tissue may decrease clinical diagnostic accuracy by generating false-positives. False-negatives are also possible if one incorrectly suspects an attenuation artifact.

In our experiment, the location of apparent "defects" resulting from attenuation was highly variable, depending on the orientation of the myocardium and the precise positioning of the breast tissue. Furthermore, an asymmetric polar map was obtained even without breast tissue due to the nonuniform attenuation of the thorax. Thus, although anterior "defects" are commonly produced by breast tissue attenuation (*8*), false "defects" appear to be possible anywhere in the polar map.

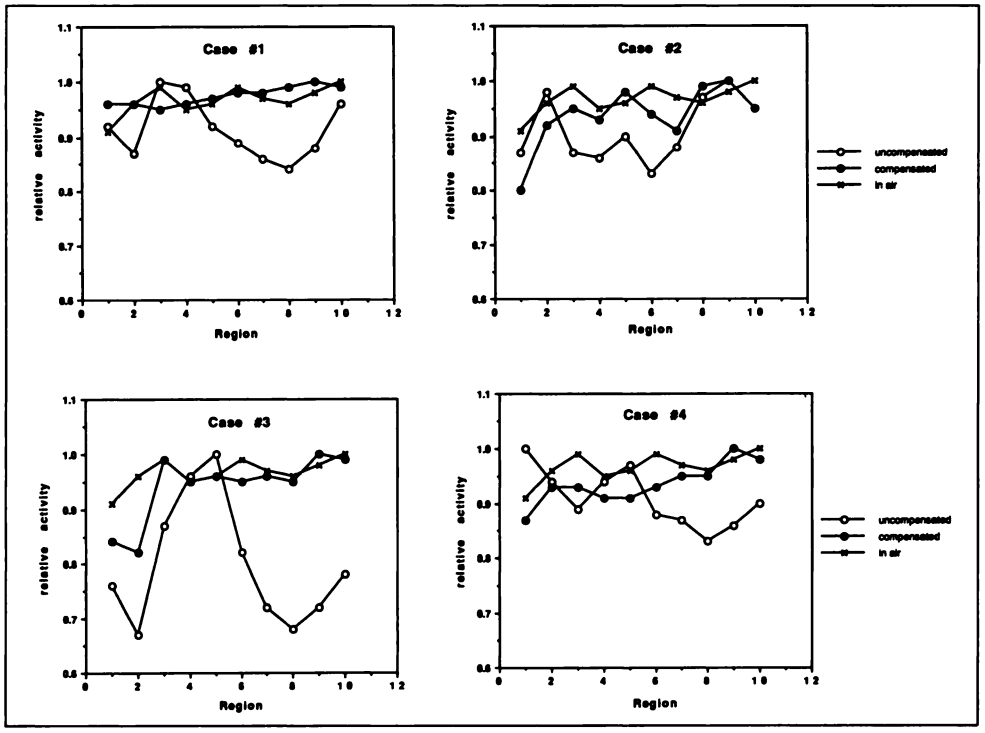

FIGURE 4. Regional semiquantitative analysis of polar maps of the myocardium phantom. The four cases shown are defined in Table 1 and the regions are defined in Figure 2. Results are given without attenuation compensation, with attenuation compensation and for the phantom "in air." Note that the "in air" data have reduced self-attenuation and thus do not provide a quantitatively correct standard for comparison.

This experiment also established that nonuniform attenuation compensation using an accurate attenuation map successfully reduces or eliminates attenuation "defects." Thus, we expect that accurate attenuation compensation will improve the diagnostic accuracy of myocardial SPECT. In particular, it is probably necessary for correct diagnosis of anterior wall defects in female patients. In contrast, attenuation compensation with an incorrect uniform attenuation map is unlikely to be helpful. First, the decreased attenuation of the lungs would be incorrectly modeled, and second, simple convex body contour models do not properly model the breasts. Concave body contours are probably measurable only with transmission CT.

The most difficult aspect of attenuation compensation is measurement of the attenuation map. Parallel-ray CT (*4,9,10*) with sheet sources has poor image resolution and count rate sensitivity. Even for a 20–30-min acquisition, relatively noisy images are produced, which may distort the SPECT study if used for attenuation compensation. However, truncation artifacts are small or nonexistent and segmentation can reduce noise (*11*). Cone-beam and fan-beam CT have substantially higher sensitivity and resolution (*12,14,15*), but the focused geometry produces truncation artifacts. Cone-beam reconstruction may have artifacts due to insufficient sampling of the three-dimensional geometry, but these artifacts, as well as truncation artifacts, are reduced with the long focal length collimator

TABLE 1
Case Definitions

Case no.	Insert orientation	Breast tissue location
	Caudal tilt from transverse plane	
1	90°	None
2	20°	Above apex
3	65°	Covering apex
4	65°	Above apex

Note: in each case, the insert was oriented approximately mid-way between anterior and left lateral.

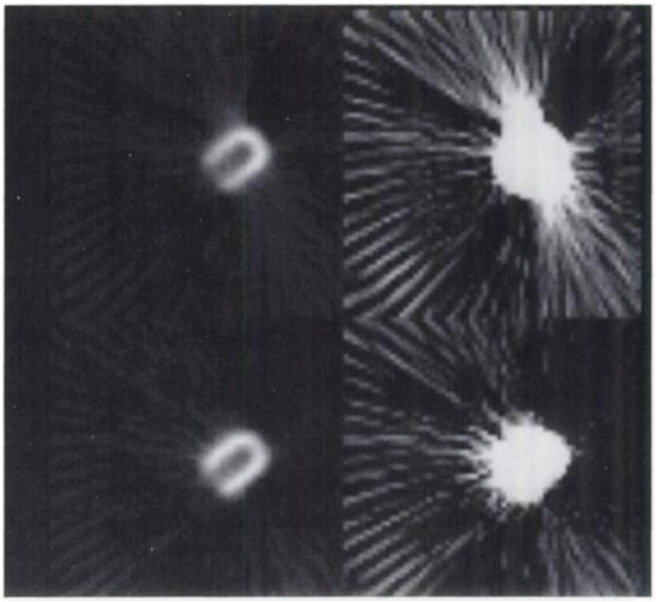

FIGURE 5. Representative reconstructed transverse slices for Case 2 prior to oblique reorientation. The upper images are uncompensated and the bottom images are attenuation compensated using the CB-CT attenuation map shown in Figure 1. In the right column, the top of the gray scale has been adjusted to 6% of the maximum count to accentuate streak artifacts.

used in this experiment. For the current experiment, the truncation artifacts were minimal, but a relatively small phantom was used. Many patients requiring myocardial imaging are much larger than our phantom and the truncation problem is more serious. For such patients, attenuation compensation of breast tissue will be difficult, and it is not yet clear which method will be best.

Nonetheless, since the theoretical utility of attenuation compensation in myocardial imaging has been established here and elsewhere (*4,6,14*), the most important remaining question is a practical one: will the improvement in diagnostic accuracy, as measured by a yet to be performed clinical experiment, justify the increased difficulty in performing attenuation compensation?

REFERENCES

1. Budinger TF, Derenzo SE, Gullberg GT, Greenberg WL, Huesman RH. Emission computed assisted tomography with single-photon and positron annihilation photon emitters. *J Comp Asst Tomogr* 1977;1:131–145.
2. Jaszczak RJ, Coleman RE, Whitehead FR. Physical factors affecting quantitative measurements using camera-based single photon emission computed tomography. *IEEE Trans Nucl Sci* 1981;28:69–80.
3. Manglos SH, Jaszczak RJ, Floyd CE, Hahn LJ, Greer KL, Coleman RE. Nonisotropic attenuation in SPECT: phantom tests of quantitative effects and compensation techniques. *J Nucl Med* 1987;28:1584–1591.
4. Tsui BMW, Gullberg GT, Edgerton ER, et al. Correction of nonuniform attenuation in cardiac SPECT imaging. *J Nucl Med* 1989;30:497–507.
5. Gillen GL, Gilmore B, Elliott AT. An investigation of the magnitude and causes of count loss artifacts in SPECT imaging. *J Nucl Med* 1991;32:1771–1776.
6. Singh M, Berggren MJ, Gustafson DE, Dewanjee MK, Bahn RC, Ritman EL. Emission computed tomography and its application to imaging of acute myocardial infarction in intact dogs using ^{99m}Tc-pyrophosphate. *J Nucl Med* 1979;20:50–56.
7. Esquerré J-P, Coca FJ, Martinez SJ, Guiraud RF. Prone decubitus: a solution to inferior wall attenuation in thallium-201 myocardial tomography. *J Nucl Med* 1989;30:398–401.
8. DePuey EG, Garcia EV. Optimal specificity of thallium-201 SPECT through recognition of imaging artifacts. *J Nucl Med* 1989;30:441–449.
9. Malko JA, VanHeertum RL, Gullberg GT, Kowalsky WP. SPECT liver imaging using an iterative attenuation correction algorithm and an external flood source. *J Nucl Med* 1986;27:701–705.
10. Bailey DL, Hutton BF, Walter PJ. Improved SPECT using simultaneous emission and transmission tomography. *J Nucl Med* 1987;28:844–851.
11. Galt JR, Cullum SJ, Garcia EV. SPECT quantification: a simplified method of attenuation and scatter correction for cardiac imaging. *J Nucl Med* 1992;33:2232–2237.
12. Manglos SH, Bassano DA, Duxbury CE, Capone RB. Attenuation maps for SPECT determined using cone beam transmission computed tomography. *IEEE Trans Nucl Sci* 1990;37:600–608.
13. Manglos SH, Bassano DA, Thomas FD. Cone-beam transmission CT for nonuniform attenuation compensation of SPECT images. *J Nucl Med* 1991; 32:1813–1820.
14. Tung C-H, Gullberg GT, Zeng GL, Christian PE, Datz FL, Morgan HT. Nonuniform attenuation correction using simultaneous transmission and emission converging tomography. *IEEE Trans Nucl Sci* 1992;39:1134–1143.
15. Manglos SH, Bassano DA, Thomas FD, Grossman ZD. Imaging of the human torso using cone beam transmission CT implemented on a rotating gamma camera. *J Nucl Med* 1992;33:150–156.
16. Lange K, Carson R. EM reconstruction algorithms for emission and transmission tomography. *J Comp Assist Tomogr* 1984;8:306–316.
17. Manglos SH. Truncation artifact suppression in cone-beam radionuclide transmission CT using maximum likelihood techniques: evaluation with human subjects. *Phys Med Biol* 1992;37:549–562.
18. Tanaka E. Toyama H, Murayama H. Convolutional image reconstruction for quantitative single photon emission computed tomography. *Phys Med Biol* 1984;29:1489–1500.
19. Manglos SH, Jaszczak RJ, Floyd CE. Weighted backprojection implemented with a non-uniform attenuation map for improved SPECT quantitation. *IEEE Trans Nucl Sci* 1988;35:625–628.
20. Harris CC, Greer KL, Jaszczak RJ, Floyd CE, Fearnow EC, Coleman RE. Technetium-99m attenuation coefficients in water-filled phantoms determined with gamma cameras. *Med Phys* 1984;11:681–685.
21. Garcia EV, Van Train K, Maddahi J, et al. Quantification of rotational thallium-201 myocardial tomography. *J Nucl Med* 1985;26:17–26.
22. Feldkamp LA, Davis LC, Kress JW. Practical cone beam algorithm. *J Opt Soc Am A* 1984;1:612–619.